

1 Cost-benefit analysis of coastal flood defence measures in the North 2 Adriatic Sea

3 Mattia Amadio¹, Arthur H. Essenfelder¹, Stefano Bagli², Sepehr Marzi¹, Paolo Mazzoli², Jaroslav Mysiak¹,
4 Stephen Roberts³

5 ¹ *Centro Euro-Mediterraneo sui Cambiamenti Climatici, Università Ca' Foscari Venezia, Italy*

6 ² *Gecosistema, Rimini, Italy*

7 ³ *The Australian National University, Canberra, Australia*

8 *Correspondence to: Arthur H. Essenfelder (arthur.essenfelder@cmcc.it)*

9 Abstract

10 The combined effect of extreme sea levels and land subsidence phenomena poses a major threat to coastal
11 settlements. Coastal flooding events are expected to grow in frequency and magnitude, increasing the
12 potential economic losses and costs of adaptation. In Italy, a large share of the population and economic
13 activities are located along the coast of the peninsula, although risk of inundation is not uniformly
14 distributed. The low-lying coastal plain of Northeast Italy is the most sensitive to relative sea level changes.
15 Over the last half a century, the entire north-eastern Italian coast has experienced a significant rise in relative
16 sea level, the main component of which was land subsidence. In the forthcoming decades, climate-induced
17 sea level rise is expected to become the first driver of coastal inundation hazard. We propose an assessment
18 of flood hazard and risk linked with extreme sea level scenarios, both under historical conditions and sea
19 level rise projections at 2050 and 2100. We run a hydrodynamic inundation model on two pilot sites located
20 in the North Adriatic Sea along the Emilia-Romagna coast: Rimini and Cesenatico. Here, we compare
21 alternative risk scenarios accounting for the effect of planned and hypothetical seaside renovation projects
22 against the historical baseline. We apply a flood damage model developed for Italy to estimate the potential
23 economic damage linked to flood scenarios and we calculate the change in expected annual damage
24 according to changes in the relative sea level. Finally, damage reduction benefits are evaluated by means of
25 cost-benefit analysis. Results suggest an overall profitability of the investigated projects over time, with
26 increasing benefits due to increased probability of intense flooding in the next future.

27 **Key-words:** coastal inundation Italy extreme sea level rise

28 **Abbreviations:** MSL (Mean Sea Level); TWL (Total Water Level); ESL (Extreme Sea Level); SLR (Sea Level
29 Rise); VLM (Vertical Land Movements); DTM (Digital Terrain Model); EAD (Expected Annual Damage)

30 1. Introduction

31 Globally, more than 700 million people live in low-lying coastal areas (McGranahan et al. 2007), and about
32 13% of them are exposed to a 100-year return period flood event (Muis et al. 2016). On average, one million
33 people located in coastal areas are flooded every year (Hinkel et al. 2014). Coastal flood risk shows an
34 increasing trend in many places due to socio-economic growth (Bouwer 2011; Jongman et al. 2012b) and land
35 subsidence (Syvitski et al. 2009; Nicholls and Cazenave 2010), but in the near future sea level rise (SLR) will
36 likely be the most important driver of increased coastal inundation risk (Hallegatte et al. 2013; Hinkel et al.
37 2014). Evidences show that global sea level has risen at faster rates in the past two centuries compared to the
38 millennial trend (Kemp et al. 2011; Church and White 2011), topping 3.2 mm per year in the last decades
39 mainly due to ocean thermal expansion and glacier melting processes (Mitchum et al. 2010; Meyssignac and
40 Cazenave 2012). According to the IPCC projections, it is very likely that, by the end of the 21st century, the
41 SLR rate will exceed that observed in the period 1971-2010 for all Representative Concentration Pathway

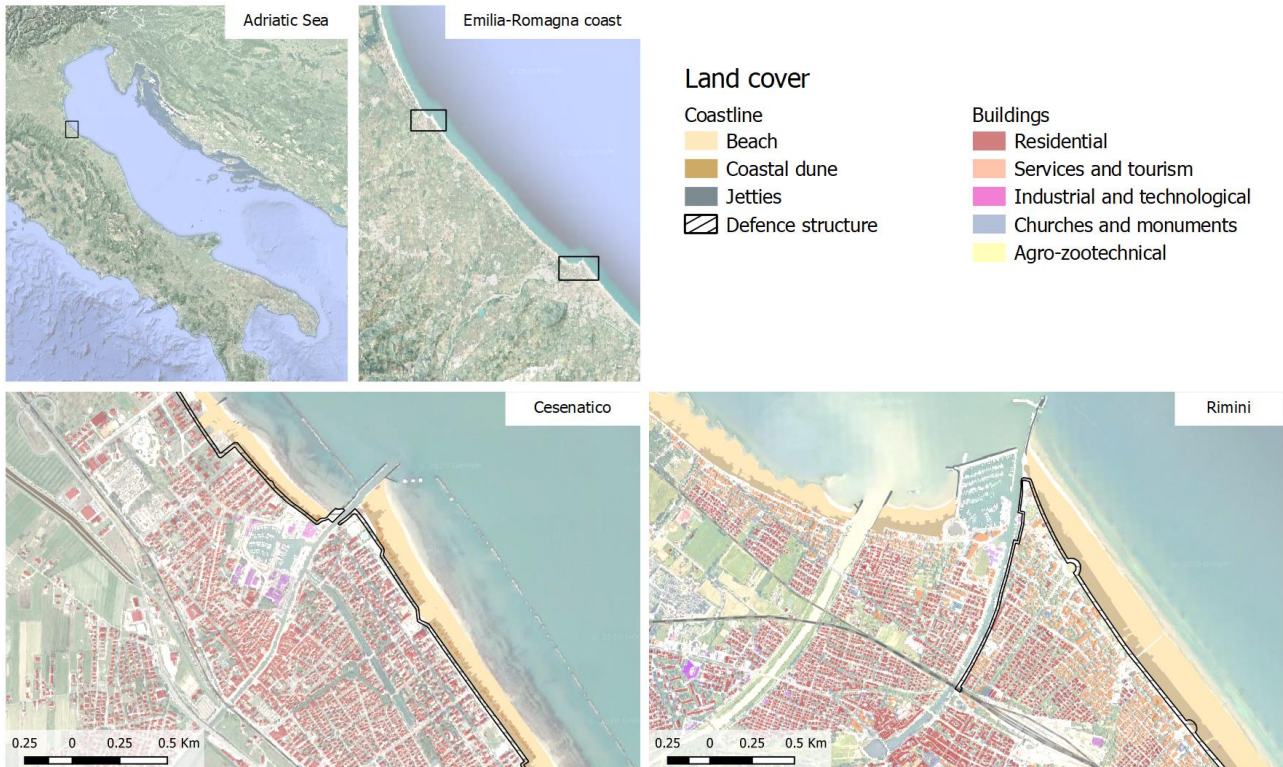
42 (RCP) scenarios (IPCC 2019); yet the local sea level can have a strong regional variability, with some places
43 experiencing significant deviations from the global mean change (Stocker et al. 2013). This is particularly
44 worrisome in regions where changes in the mean sea level (MSL) are more pronounced, considering that
45 even small increases of MSL can drastically change the frequency of extreme sea level (ESL) events, leading
46 up to situations where a 100-year event may occur several times per year by 2100 (Carbognin et al. 2009,
47 2010; Vousdoukas et al. 2017, 2018; Kirezci et al. 2020). Changes in the frequency of extreme events are likely
48 to make existing coastal protection inadequate in many places, causing a large part of the European coasts to
49 be exposed to flood hazard. Under these premises, coastal floods threaten to trigger devastating impacts on
50 human settlements and activities (Lowe et al. 2001; McInnes et al. 2003; Vousdoukas et al. 2017). In this
51 context, successful coastal risk mitigation and adaptation actions require accurate and detailed information
52 about the characterisation of coastal flood hazard and the performance of alternative coastal defence options.
53 Cost-benefit analysis (CBA) is widely used to evaluate the economic desirability of a disaster risk reduction
54 (DRR) project (Jonkman et al. 2004; Mechler 2016; Price 2018). CBA helps decision-makers in evaluating the
55 efficacy of different adaptation options (Kind 2014; Bos and Zwaneveld 2017).

56 In this study, we estimate the benefits of coastal renovation projects along the coast of Emilia-Romagna
57 region (Italy) in terms of avoided economic losses from ESL inundation events under both current and
58 future conditions. We select two coastal cities as case study areas: i) Rimini, a touristic hotspot that is
59 currently implementing a seafront renovation project; and ii) Cesenatico, a coastal city that could benefit
60 from similar measures in addition to existing defence mechanisms. We design worst-case scenarios of ESL
61 resulting from the combination of the maximum levels of mean sea level, vertical land movement, storm
62 surge, tide, and wave setup to verify the effectiveness of the above-mentioned coastal defence structures in
63 reducing flood hazard and related impacts over the urban area. To do that, first we employ the 2D-
64 hydrodynamic ANUGA model (Roberts et al. 2015) for simulating coastal inundation associated with ESL
65 scenarios over the two case study areas. The scenarios are calculated by combining probabilistic data from
66 historical ESL events with the estimates of relative mean sea level (RMSL) change for those locations. ~~RMSL~~
67 ~~change accounts for both the eustatic global rise and the locally measured vertical land movement effect.~~
68 Each inundation scenario simulated by the hydrodynamic model is ~~translated~~ evaluated in terms of direct
69 economic impacts over residential areas using a locally-calibrated damage model. The combination of
70 different risk scenarios in a CBA framework allows to evaluate the economic benefits brought by the project
71 implementation in terms of avoided direct flood losses up to the end of the century.

72 2. Area of study

73 Located in the central Mediterranean Sea, the Italian peninsula has more than 8,300 km of coasts, hosting
74 around 18% of the country population, numerous towns and cities, industrial plants, commercial harbours
75 and touristic activities, as well as cultural and natural heritage sites. Existing country-scale estimates of SLR
76 impacts up to the end of this century helps to identify the most critically exposed coastal areas of Italy
77 (Lambeck et al. 2011; Bonaduce et al. 2016; Antonioli et al. 2017; Marsico et al. 2017). About 40% of the
78 country's coastal perimeter consist of a flat coastal profile (ISPRA 2012), potentially more vulnerable to the
79 impacts of ESL events. The North Adriatic coastal plain is acknowledged to be the largest and most
80 vulnerable location to extreme coastal events due to the shape, morphology and low bathymetry of the
81 Adriatic sea basin, which cause water level to increase relatively fast during coastal storms (Carbognin et al.
82 2010; Ciavola and Coco 2017; Perini et al. 2017). The ESL here is driven mainly by astronomical tide, ranging
83 about one meter in the northernmost sector; and meteorological forcing, such as low pressure, seiches and
84 prolonged rotational wind systems, which are the main trigger of storm surge in the Adriatic basin

85 (Vousdoukas et al. 2017; Umgiesser et al. 2020). In addition to that, all the coastal profile of the Padan plain
 86 shows relatively fast subsiding rates, partially due to natural phenomena, but in large part linked to human
 87 activities (Carbognin et al. 2009; Perini et al. 2017; Meli et al. 2021). As a contributing factor to coastal flood
 88 risk, the intensification of urbanization has led to increased exposure along the Adriatic coast during the last
 89 50 years, with many regions building over half of the available land within 300 meters from the shoreline
 90 (ISPRA 2012). Figure 1 shows the location of the two case study areas, Cesenatico and Rimini, along with
 91 land-cover maps showing the position of coastal defences accounted in this study.



92
 93 **Figure 1.** Case-study locations along the Emilia-Romagna coast: Cesenatico and Rimini. The coastal defence
 94 structure assessed in this study are shown in black. Buildings' footprint data from Regional Environmental
 95 Agency (ARPA) 2020. Basemap © Google Maps 2020.

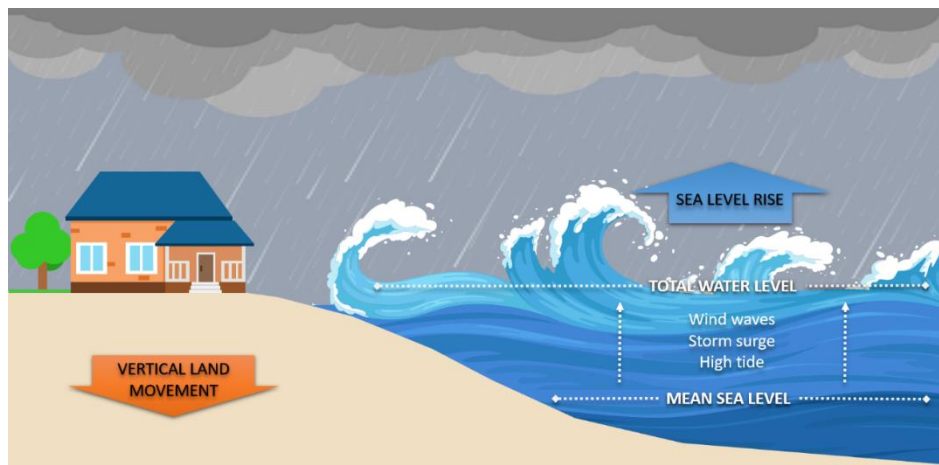
96 The number of ESL events reported to cause impacts along the Emilia-Romagna coast shows a steady
 97 increase since the second half of the past century (Perini et al. 2011), which is in part explained by to the
 98 socio-economic development of the coast exposing increasing asset to flood risk. The landscape along the 130
 99 km regional coastline is almost flat, the only relief being old beach ridges, artificial embankments and a
 100 small number of dunes. The coastal perimeter is delineated by a wide sandy beach that is generally
 101 protected by offshore breakwaters, groins and jetties. The land elevation is often close to (or even below) the
 102 MSL, while the coastal corridor is heavily urbanised. Cesenatico has about 26,000 residents, while Rimini has
 103 150,000. The towns have a strong touristic vocation, hosting large beach resort and bathing facilities along
 104 the beach and hundreds of hotels and rental housing located just behind the seaside. Both places have been
 105 affected by coastal storms resulting in flooding of buildings and activities, beach erosion and regression of
 106 the coastline. The most recent inundation events were observed in March 2010, November 2012 and
 107 February 2015. The 2015 event was one of the most severe ever recorded, with ESL values corresponding to a
 108 probability of once in 100 years. It caused severe damages along the whole regional coast and, in some
 109 locations, required the evacuation of people from their houses; many buildings and roads were covered by
 110 sand brought by the flood wave; touristic infrastructures near the shore were seriously damaged, and some

111 port channels overflowed the surrounding areas. The economic impact of the event was estimated topping
112 7.5 M Eur (Perini et al. 2015).

113 3. Methodology

114 3.1 Components of the analysis

115 Coastal inundation is caused by an increase of total water level (TWL), most often associated to extreme sea
116 level (ESL) events, which are often generated by a combination of high astronomical tide and meteorological
117 drivers such as storm surge and wind waves (Figure 2). Estimates of ESL are obtained for the North
118 Adriatic up to year 2100 by combining reference hazard scenarios derived from historical records with
119 regionalised projections of SLR (Vousdoukas et al. 2017) and local vertical land movements (VLM) rates
120 (Carbognin et al. 2009; Perini et al. 2017). Four ESL frequency scenarios, namely once in 1, 10, 100 and 250
121 years, are considered. The hydrodynamic model ANUGA is applied to simulate the inundation of land areas
122 during ESL accounting for individual components (storm surge, tides and waves). Land morphology and
123 exposure of coastal settlements are described by high-resolution DTM and bathymetry, in combination with
124 land use and buildings footprints. The effect of hazard mitigation structures (both designed and under
125 construction) are explicitly accounted in the “defended” simulation scenario, in contrast to the baseline
126 scenario, where only existing defence structures (groins, jetties, breakwaters and sand dunes) are accounted.



127
128 **Figure 2.** Components of the analysis for extreme sea level events: total water level is the sum of maximum
129 tide, storm surge and wind waves over mean sea level. Vertical land movement and eustatic sea level rise
130 affects the mean sea level on the long run.

131 3.2 Vertical Land Movement

132 Vertical land movements result from a combination of slow geological processes such as tectonic activity and
133 glacial isostatic adjustment (Peltier 2004; Peltier et al. 2015), and medium-term phenomena, such as sediment
134 loading and soil compaction (Carminati and Martinelli 2002; Lambeck and Purcell 2005). The latter can
135 greatly oversize geological processes at local scale (Wöppelmann and Marcos 2012); in particular, faster
136 subsidence occurs in presence of intense anthropogenic activities such as water withdrawal and natural gas
137 extraction (Teatini et al. 2006; Polcari et al. 2018). Most of the peninsula shows a slow subsiding trend,
138 although with some local variability. An estimate of VLM rates due to tectonic activity has been derived
139 from studies conducted in Italy (Lambeck et al. 2011; Antonioli et al. 2017; Marsico et al. 2017; Solari et al.
140 2018). The North Adriatic coastal plain shows the most intense long-term geological subsidence rates (about
141 1 mm per year), increasing North to South. Yet in the last decades these rates were often greatly exceeded by

142 ground compaction rates observed by multi-temporal SAR Interferometry (Gambolati et al. 1998; Antonioli
143 et al. 2017; Polcari et al. 2018; Solari et al. 2018). Observed subsidence is about one order of magnitude faster
144 where the aquifer system has been extensively exploited for agricultural, industrial and civil use since the
145 post-war industrial boom. From the 1970s, however, with the halt of groundwater withdrawals,
146 anthropogenic drivers of subsidence has been strongly reduced or stopped (Carbognin et al. 2009).
147 Nonetheless, subsidence still continues at much faster rates than expected from natural phenomena (Teatini
148 et al. 2005). Geodetic surveys carried out from 1953 to 2003 along the Ravenna coast provide evidence of a
149 cumulative land subsidence exceeding 1 m at some sites due to gas extraction activities. Average subsidence
150 rates observed for 2006-2011 along the Emilia-Romagna coast are around 5 mm/yr, exceeding 10 mm/yr in
151 the back shore of the Cesenatico and Rimini areas and topping 20-50 mm/yr in Ravenna (Carbognin et al.
152 2009; Perini et al. 2017). Based on these current rates, we assume an average fixed annual VLM of 5 mm in
153 both Cesenatico and Rimini up to the end of the century. This remarkable difference between natural VLM
154 rates and observations would produce a dramatic effect on the estimated SLR scenarios: at present rates,
155 Rimini would see an increase of MSL by 0.15 m in 2050 and more than 0.4 m in 2100 independently from
156 eustatic SLR. Since these rates are connected with human activity, it is not possible to foresee exactly how
157 they will change in the long term.

158 3.3 Sea Level Rise

159 The long availability of tide gauge data along the North Adriatic coast allows to assess the eustatic changes
160 in MSL during the last century, estimated to be +1.3 mm/year (Scarascia and Lionello 2013). This is
161 consistent with published values for the Mediterranean Sea (Tsimplis and Rixen 2002; Tsimplis et al. 2008)
162 and the Adriatic Sea (Carbognin et al. 2009; Tsimplis et al. 2012). ~~Records from the gauge station of Marina di~~
163 ~~Ravenna show an eustatic rise of 1.2 mm per year from 1890 to 2007, in good agreement with the eustatic~~
164 ~~rise measured at other stations in the Mediterranean Sea~~. The projections of future MSL account for sea
165 thermal expansions from four global circulation models, estimated contributions from ice-sheets and glaciers
166 (Hinkel et al. 2014) and long-term subsidence projections (Peltier 2004). The ensemble mean is chosen to
167 represent each RCP for different time slices. The increase in the central Mediterranean basin is projected to
168 be approximately 0.2 m by 2050 and between 0.5 and 0.7 m by 2100, compared to historical mean (1970-2004)
169 (Vousdoukas et al. 2017). As agreed with stakeholders, our analysis considers the intermediate emission
170 scenario RCP 4.5, projecting an increase in MSL of 0.53 m at 2100. It must be noted that these projections,
171 although downscaled for the Adriatic basin, do not account for the peculiar continental characteristics of the
172 shallow northern Adriatic sector, where the hydrodynamics and oceanographic parameters partially depend
173 on the freshwater inflow (Zanchettin et al. 2007).

174 3.4 Tides and meteorological forcing

175 Storm surge and wind waves represent the largest contribution to TWL during an ESL event. An estimation
176 of these components is obtained for the two coastal sites from the analysis of tide gauge and buoy records,
177 and from the description of historical extreme events presented in local studies (Perini et al. 2011, 2012, 2017;
178 Masina et al. 2015; Armaroli and Duo 2018). This area is microtidal: the mean neap tidal range is 30–40 cm,
179 and the mean spring tidal range is 80–90 cm. Most storms have a duration of less than 24 h and a maximum
180 significant wave height of about 2.5 m. During extreme cyclonic events, the sequence of SE wind (*Sirocco*)
181 piling the water North and E-NE wind (*Bora*) pushing waves towards the coast can generate severe
182 inundation events, with significant wave height ranging 3.3 – 4.7 m and exceptionally exceeding 5.5 m
183 (Armaroli et al. 2012). Fifty significant events have been recorded from 1946 to 2010 on the ER coast, with
184 half of them causing severe impacts along the whole coast and 10 of them being associated with important

185 flooding events (Perini et al. 2017). The most severe events are found when strong winds blow during
186 exceptional tide peaks, most often happening in late autumn and winter. The event of November 1966
187 represents the highest ESL on records, causing significant impacts along the regional coast: the recorded
188 water level was 1.20 m above MSL, and wave heights offshore were estimated around 6–7 m (Perini et al.
189 2011; Garnier et al. 2018). The whole coastline suffered from erosion and inundation, especially in the
190 province of Rimini. Atmospheric forcing shown significant variability for the period 1960 onwards (Tsimplis
191 et al. 2012), but there is no strong evidence supporting a significant change in ~~marine trend-storminess~~
192 ~~frequency or severity~~ for the ~~next-near~~ future (Lionello 2012; Lionello et al. 2017, 2020; Zanchettin et al. 2020).
193 Thus, ~~in our model~~ we assume ~~the frequency and intensity of~~ meteorological ~~events forcing~~ to remain the
194 same up to 2100.

195 3.5 Terrain morphology and coastal defence structures

196 Reliable bathymetries and topography are required in order to run the hydrodynamic modelling at the local
197 scale. Bathymetric data for the Mediterranean Sea were obtained from the European Marine Observation
198 and Data Network (EMODnet) at 100 m resolution. The description of terrain morphology comes from the
199 official high-resolution LIDAR DTM (MATTM, 2019). First, we combined the coastal dataset (2 m resolution
200 and vertical accuracy of ± 0.2 m), and the inland dataset (1 m resolution and vertical accuracy ± 0.1 m) into
201 one seamless layer. Then, the DTM is supplemented with geometries of existing coastal protection elements
202 such as jetties, groins and breakwaters obtained from the digital Regional Technical Map. In Rimini, the
203 *Parco del Mare* (Figure 3) is an urban renovation project which aims to improve the seafront promenade: the
204 existing road and parking lots are converted into an urban green infrastructure consisting of a concrete
205 barrier covered by vegetated sandy dunes with walking paths. This project also acts as a coastal defence
206 system during extreme sea level events. The barrier rises 2.8 meters along the southern section of the town,
207 south of the marina; no barrier is planned on the northern coastal perimeter. The *Parco del Mare* project is
208 currently under construction and has been taken in account in the evaluation of the “defended” scenarios by
209 adding the barrier to the DTM.



210
211 **Figure 3.** Prototype design of Parco del Mare project in Rimini. Adapted from JDS Architects.

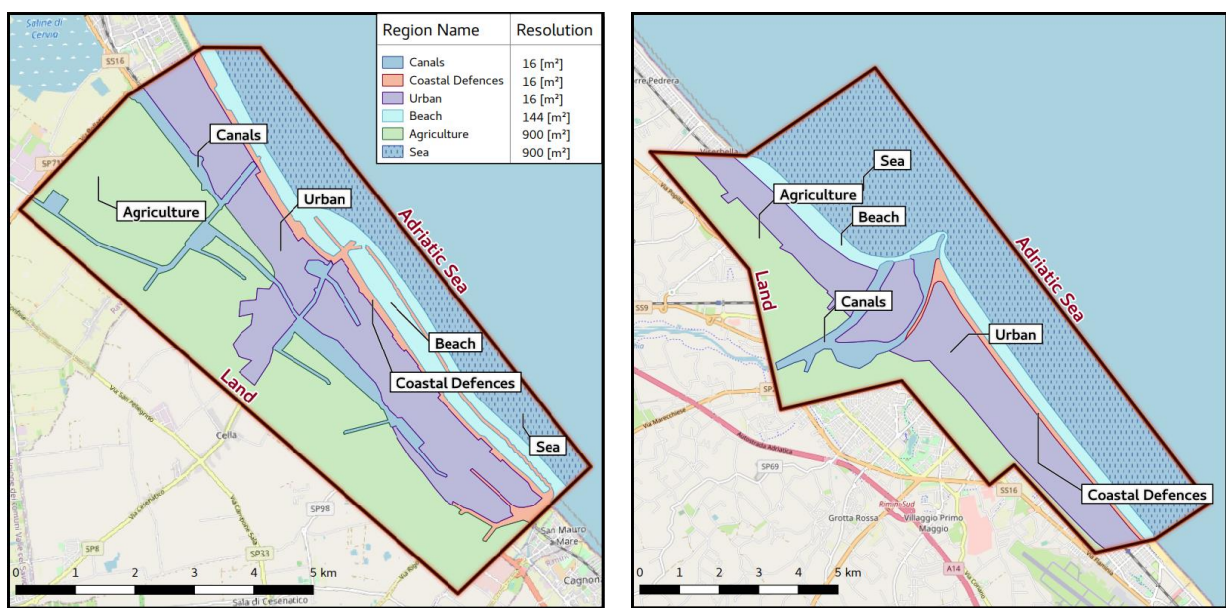
212 In Cesenatico, the existing defence structures include a moving barrier system (*Porte Vinciane*) located on the
213 port channel, coupled with a dewatering pump which discharge the meteoric waters in the sea. The barriers
214 close automatically if the TWL surpasses 1 meter over the mean sea level, preventing floods in the historical
215 centre up to 2.2 meters of TWL. Additional defence structures include the winter dunes, which consist of a
216 2.2 meter-tall intermittent, non-reinforced sand barrier. In the defended scenario, we envisage a coastal
217 defence structure similar to Rimini’s *Parco del Mare* project, spanning both North and South of the port
218 channel with a total length of 7.8 km. A proper setup of the inundation model required to first perform some
219 manual editing of the DTM using additional reference data (i.e. on-site observations or aerial photography)

220 in order to produce an elevation model that realistically represent the land morphology and associated water
 221 dynamics (e.g. removal of non-existent sink holes). Bridges and tunnels are the most critical elements that
 222 required DTM correction in order to avoid misrepresentations of the water flow routing.

223 3.6 Inundation modelling

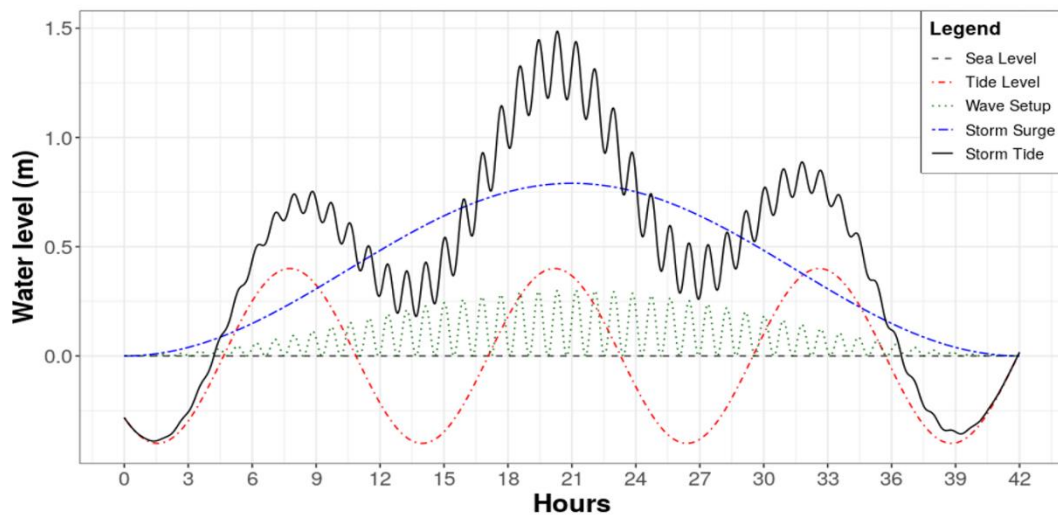
224 ~~At the local scale, hydrodynamic models represent an efficient compromise between hydrostatic and~~
 225 ~~hydraulic models, being able to perform realistic simulations of inundation phenomena and to obtain~~
 226 ~~detailed information about the hazard features, while requiring a relatively fast setup and reasonable~~
 227 ~~computational effort.~~ In this study we use ANUGA, a 2D hydrodynamic model ~~originally developed to~~
 228 ~~simulate tsunami events, which is also~~ suitable for the simulation of ~~hydrologic phenomena~~ flooding events
 229 ~~such as resulting from~~ riverine peak flows and storm surges (Roberts 2020). Being a 2D hydrodynamic
 230 model, ANUGA does not resolve vertical convection, waves breaking or 3D turbulence (e.g. vorticity), thus
 231 it ~~does~~ not accounting for the swash component of wave runup. The fluid dynamics in ANUGA is based on
 232 a finite-volume method for solving the shallow water wave equations, thus being based on continuity and
 233 simplified momentum equation. ~~ANUGA~~ The model includes also an operator module that simulates the
 234 removal of sand associated with over-topping of a sand dune by sea waves, which is applied to explore
 235 scenarios where a sand dune barrier provides protection for the land behind. The operator simulates the
 236 erosion, collapse, fluidisation and removal of sand from the dune system (Kain et al. 2020); the dune erosion
 237 mechanism relies on a relationship based on Froehlich (2002). This option is enabled only in the undefended
 238 scenario for Cesenatico, where non-reinforced sand dunes are prone to erosion.

239 The case study areas are represented by an irregular triangular mesh in which water level, water depth and
 240 horizontal momentum are computed. The size of the triangles is variable within the mesh, thus allowing or a
 241 better representation in regions of particular interest, such as along the coastline, in urban areas, and inside
 242 the canals. Six different regions are used in each case study to define different triangular mesh resolution,
 243 varying from higher resolution areas of 16 m² for canals and coastal defence structures, to lower resolution
 244 areas of 900 m² for sea areas. Figure 44 presents the considered regions and the respective resolutions for the
 245 case study cities. The resulting irregular mesh counts with 636,938 triangles for the Cesenatico case study,
 246 and 1,198,604 triangles for the Rimini case study.



248 [Figure 4. The definition of simulation domain definition](#) for the cities of Rimini (on the left) and Cesenatico
249 [\(on the right\).](#)

250 [Boundary conditions are used to specify the water level dynamics \(i.e. forcing term\) along the Adriatic Sea](#)
251 [boundary margin of each case study area to specify the water level dynamics \(i.e. forcing term\) in ANUGA's](#)
252 [domain. Based on these conditions, the model, then, computes the total water level insisting on the coast,](#)
253 [the resulting water depth of inundation, and the horizontal momentum on an irregular triangular grid based](#)
254 [on the provided forcing conditions. Figure 55 shows how boundary conditions are set-up in ANUGA during](#)
255 [a theoretical storm tide event for an example case of a once-in-10 years return period \(additional setups for](#)
256 [other RPs can be found in Annex 1\). Each of the components shown in Figure-5 is considered independently,](#)
257 [according to the intensity \(i.e. water level\) and duration of the respective storm tide event, and added to](#)
258 [generate the black continuous line representing the storm tide level \(or total water level, TWL\) as a](#)
259 [boundary condition in ANUGA. ANUGA includes also an operator module that simulates the removal of](#)
260 [sand associated with over topping of a sand dune by sea waves, which is applied to explore scenarios where](#)
261 [a sand dune barrier provides protection for the land behind. The operator simulates the erosion, collapse,](#)
262 [fluidisation and removal of sand from the dune system \(Kain et al. 2020\); the dune erosion mechanism relies](#)
263 [on a relationship based on Froehlich \(2002\). This option is enabled only in the undefended scenario for](#)
264 [Cesenatico, where non reinforced sand dunes are prone to erosion.](#)



265 **Figure 55.** Total Water Level (black) as a sum of tide (red), storm surge (blue) and wave setup (green) for
266 ESL scenario 1 in 10 years. [Additional figures for all RPs are found in Annex 1.](#)
267

268 In our application, we estimate the TWL on the coastland at every timestep as the sum of extreme values for
269 storm surge level (SS), wave setup (Ws), and max tide (T_{max}), ~~as shown in Figure 45.~~ Storm surge peak is
270 set to coincide with the tidal peak at the mid of the event, thus producing a maximum TWL value. As
271 considered, our approach is precautionary as it provides worst-case scenario ESL values. The components of
272 TWL are obtained from existing probabilistic analysis of extreme events conducted on the regional coast
273 (Perini et al. 2016, 2017) and later adopted by the Regional Environmental Agency to define the official
274 coastal flood hazard zones (ARPAE 2019). The probability of occurrence for ESL scenarios is expressed in
275 terms of return period (RP), which is the estimated average time interval between events of similar intensity,
276 accounting for all variables combined. [The high tide contribution grows from 0.40 m to 0.45 m, while wave](#)
277 [setup near the shore ranges from 0.22 m to 0.65 m. We select the scenario RP 250 years as the upper](#)
278 [boundary of hazard intensity, considering all components of TWL to reach their most extreme values and](#)
279 [summing up to +2.5 meters over MSL. The maximum tidal excursion is 0.8-0.9 m, while wave setup near the](#)

280 ~~shore can range from 0.22 to 0.65 m. For RP 250, TWL hits 2.5 meters as all components reach their most~~
 281 ~~extreme values.~~ Additional details are wave period (Wp , in seconds) and event duration ($Time$, in hours),
 282 required for the hydrodynamic simulation of coastal flooding events and the determination of the maximum
 283 extent of inland water propagation. Both variables are obtained from ~~existing~~ analysis of observations
 284 recorded during historical ESL events on the coast of Emilia-Romagna records from 1946 to 2010 (Perini et al.
 285 2011), ~~matched with the probabilistic distribution of RP scenarios (Armaroli et al. 2012; Armaroli and Duo~~
 286 2018). In our scenarios, wave direction is set to be oriented perpendicular to the coast. Table 1 summarizes
 287 the ESL components according to the four probability scenarios ~~identified from local historical records~~
 288 (Perini et al. 2017). The output of the simulation consists of maps representing flood extent, water depth and
 289 momentum at every time step (1 second), projected on the high-resolution DTM grid.

290 **Table 1.** components of TWL during an ESL event under historical conditions and projected conditions (2050
 291 and 2100), accounting for both eustatic SLR (RCP 4.5) and average VLM rate.

RP (years)	Extreme event features				Historical	2050			2100		
	SS (m)	T_{max} (m)	W_s (m)	$Time$ (h)	TWL (m)	SLR (m)	VLM (m)	TWL (m)	SLR (m)	VLM (m)	TWL (m)
1	0.60	0.40	0.22	32	1.22	0.14	0.19	1.55	0.53	0.44	2.219
10	0.79	0.40	0.30	42	1.549	0.14	0.19	1.82	0.53	0.44	2.546
100	1.02	0.40	0.39	55	1.81	0.14	0.19	2.14	0.53	0.44	2.78
250	1.40	0.45	0.65	75	2.50	0.14	0.19	2.83	0.53	0.44	3.547

292
 293 ANUGA takes into account the boundary conditions specified in Table 1 and dynamically shown in Figure 5
 294 to simulate the flood dynamics within the domain, such as water flowing through canals and the flooding of
 295 land areas. For each return period scenario, a different idealized hypothetical ESL-storm-tide event is designed
 296 in order to match the maxima level of tide and surge (following the worst-case scenario assumption, as
 297 previously mentioned). These idealized storm-tide-synthetic events are designed assuming trigonometric
 298 functional forms describing the oscillation of water level due to the different components defining ESL (Boon
 299 2004; Fuhrmann et al. 2019; Familkhalili et al. 2020) (CITATIONS?). Each component, then, has a different
 300 period and magnitude, to reflect specific contributions of each component. Regarding the wave component,
 301 since ANUGA is a 2D model that cannot simulate wave breaking and the swash component of wave runup,
 302 we simulate just the wave setup component based on values reported in regional studies (Perini et al. 2012,
 303 2016) using data obtained from the literature (CITATION?). The wave setup is a relevant component of the
 304 total water level by contributing to the flood dynamics due to the momentum of waves, particularly when
 305 directed inlands (Melet et al. 2020) (CITATION?). We consider wave setup as a function of the intensity of
 306 the storm surge level, as shown by the green dashed line in Figure 5. The maximum wave setup level is
 307 designed to coincide with the timing of maximum storm tide level, following the assumption of worst-case
 308 scenario, while wave direction is aligned with the storm surge direction, thus being perpendicular to the
 309 coastline.

310 3.7 Risk modelling and Expected Annual Damage

311 Direct damage to physical asset is estimated using a customary flood risk assessment approach originally
 312 developed for fluvial inundation, which is adapted to coastal flooding assuming that the dynamic of impact
 313 from long-setting floods depends on the same factors, namely: 1) hazard magnitude, and 2) size and value of
 314 exposed asset. Indirect economic losses due to secondary effects of damage (e.g. business interruption) are
 315 excluded from the computation. Hazard magnitude can be defined by a range of variables, but the most
 316 important predictors of damage are water depth and the extension of the flood event (Jongman et al. 2012a;

317 Huizinga et al. 2017). Land cover definitions and buildings footprints help to estimate the exposed capital
 318 including residential buildings, commercial and industrial activities, infrastructures, historical and natural
 319 sites. The characterization of exposed asset is built from a variety of sources, starting from land use and
 320 buildings footprints obtained from the Regional Environmental Agencies geodatabases and the Open Street
 321 Map database (Geofabrik GmbH 2018). Additional indicators about buildings characteristics are obtained
 322 from the database of the 2011 Italian Census (ISTAT 2011), while mean construction and restoration costs per
 323 building types are obtained from cadastral estimates (CRESME 2014). The asset representation is static, thus
 324 not accounting for changes in land use nor population density, while allowing for the direct comparison of
 325 hazard mitigation options' results. A depth-damage function was previously validated on empirical records
 326 (Amadio et al. 2019) and then applied in order to translate each hazard scenario into an estimate of economic
 327 risk, measured as a share of total exposed value. The damage function applies only to residential and mixed-
 328 residential buildings, the area of which represents about 93% of total exposed footprints; other types (such as
 329 harbour infrastructures, industrial, commercial, historical monuments and natural sites) are excluded from
 330 risk computation. Abandoned or under-construction buildings are also excluded from the analysis. To avoid
 331 overcounting of marginally-affected buildings, we set two threshold conditions for damage calculation:
 332 flood extent must be greater than or equal to 10 m², and maximum water depth greater than or equal to 10
 333 cm. The damage/probability scenarios are combined together as Expected Annual Damage (EAD). EAD is
 334 the damage that would occur in any given year if damages from all flood probabilities were spread out
 335 evenly over time; mathematically, EAD is the integration of the flood risk density curve over all probabilities
 336 (Olsen et al. 2015), as in equation 1.

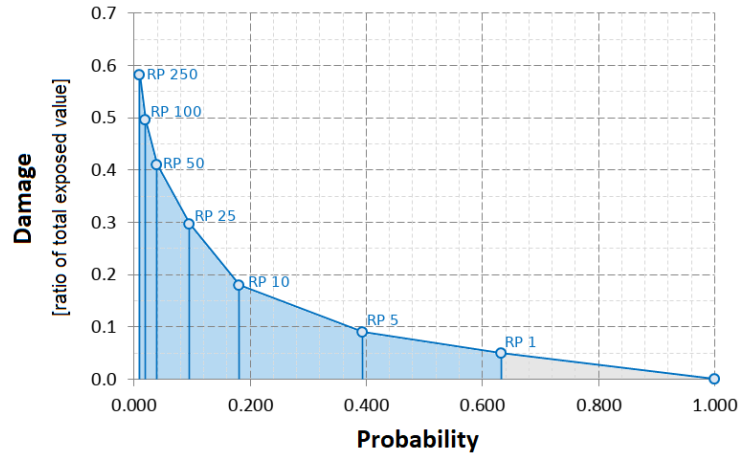
$$EAD = \int_0^1 D(p) dp \quad (1)$$

337 The integration of the curve can be solved either analytically or numerically, depending on the complexity of
 338 the damage function $D(p)$. Several different methods for numerical integration exist; we use an approach
 339 where EAD is the sum of the product of the fractions of exceedance probabilities by their corresponding
 340 damages (Figure 65). We calculate $D(p)$, which is the damage that occurs at the event with probability p , by
 341 using the depth-damage function for each hazard scenario. The exceedance probability of each event (p) is
 342 calculated based on exponential function as shown in equation 2.

$$p = 1 - e^{\left(\frac{-1}{RP}\right)} \quad (2)$$

343 Events with a high probability of occurrence and low intensity (below RP 1 year) are not simulated, as they
 344 are assumed to not cause significant damage. This is consistent with the historical observations for the case
 345 study area, although this assumption could change with increasing MSL.

Figure 665. Schematic representation of the numerical integration of the damage function $D(p)$ with respect to the exponential probability of the hazard events. Damage (Y axis) represents the ratio of damage to the total exposed value estimated up to the most extreme scenario (RP 250 years). Events with a probability of occurrence higher than once in a year are expected to not cause damage (grey area).



346 3.8 Cost-Benefit Analysis

347 A CBA should include a complete assessment of the impacts brought by the implementation of the hazard
 348 mitigation option, i.e. direct and indirect, tangible and intangible impacts (Bos and Zwaneveld 2017). The
 349 project we are considering, however, has not been primarily designed for DRR purpose: instead, it is meant
 350 as an urban renovation project which aims to consolidate the touristic vocation of the area, to improve the
 351 quality of life and the urban environment (Comune di Rimini 2018). This implies some large indirect effects
 352 on the whole area, most of which are not strictly related to disaster risk management and, overall, very
 353 difficult to estimate ex-ante. Our evaluation focuses only on the benefits that are measurable in terms of
 354 direct flood losses reduction. Regarding the implementation costs, the CBA accounts for the initial
 355 investment required for setting up the adaptation measure, and operational costs through time. According to
 356 the *Parco del Mare* project funding documentation (Comune di Rimini 2019a, b, 2020, 2021a, b), the total cost
 357 of the project (to be completed during 2021) is 33.3 M Eur, corresponding to 5.55 M Eur per Km of length. No
 358 information is available about maintenance costs of the opera, but given the nature of the project (static
 359 defense with low structural fragility), we assume they will be rather small compared to the initial
 360 investment. Ordinary annual maintenance costs are accounted as 0.1% of the total cost of the project. The
 361 same costs are assumed for the hypothetical barrier in Cesenatico, resulting in an initial investment cost of
 362 43.3 M. Costs and benefit occurring in the future periods need to be discounted, as people put higher value
 363 on the present (Rose et al., 2007). This is done by adjusting future costs and benefits using an annual
 364 discount rate (r). We chose a variable rate of $r = 3.5$ for the first 50 years and $r = 3$ from 2050 onward (Lowe
 365 2008). A sensitivity analysis of discount rate is included in Annex 42. The three main decision criteria used in
 366 CBA for project evaluation are the Net Present Value (NPV), the Benefit/Cost Ratio (BCR) and the payback
 367 period. The NPV is the sum of Expected Annual Benefits (B) up to the end of the time horizon, discounted,
 368 minus the total costs for the implementation of the defense measure, which takes into account initial
 369 investment plus discounted annual maintenance costs (C). In other words, the NPV of a project equals the
 370 present value of the net benefits ($NB_i = B_i - C_i$) over a period of time (Boardman et al. 2018), as in equation
 371 (3):

$$NPV = PV(B) - PV(C) = \sum_{t=0}^n \frac{NB_t}{(1+r)^t} \quad (3)$$

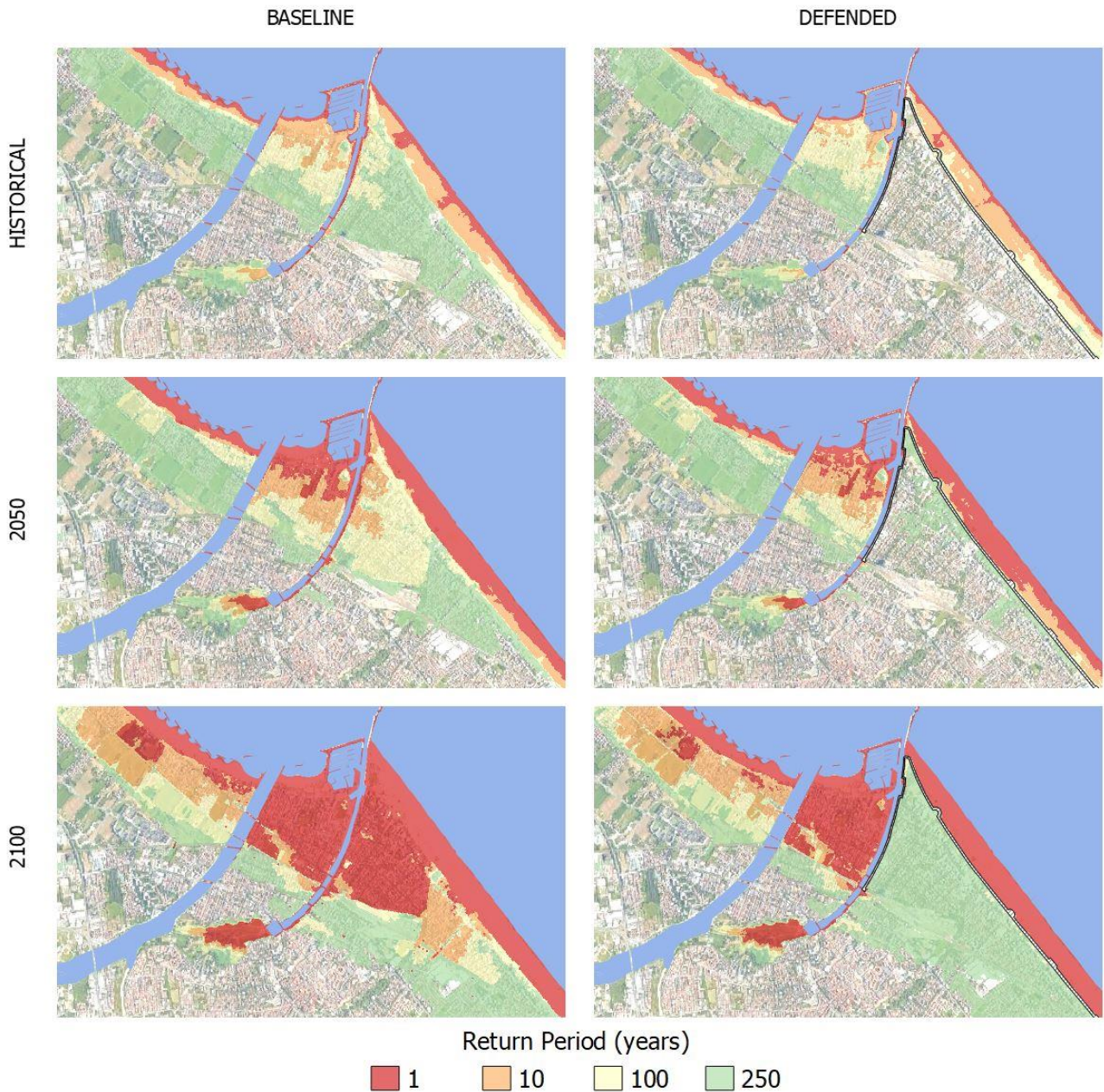
372 Positive NPV means that the project is economically profitable. The BCR is instead the ratio between the
 373 benefits and the costs; a BCR larger than 1 means that the benefits of the project exceed the costs on the long

374 term and the project is considered profitable. The payback period is the number of years required for the
375 discounted benefits to equal the total costs.

376 4. Results

377 4.1 Inundation scenarios

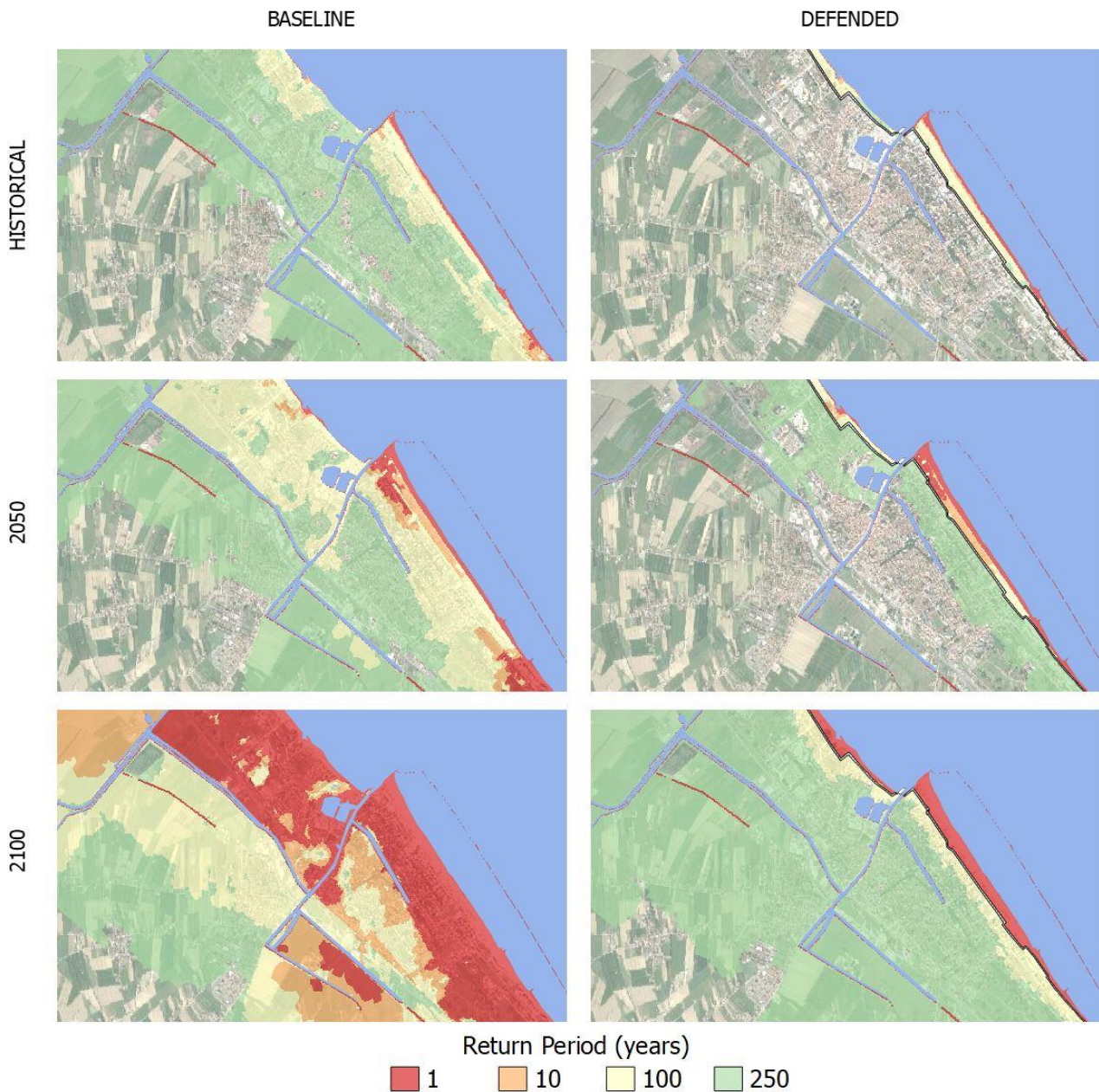
378 Once the setup is completed, the hydrodynamic model performs relatively fast: each simulation is carried at
379 half speed compared to real time, requiring about 24 hours to simulate a 12 h event. Parallel simulations for
380 the same area can run on a multicore processor, improving the efficiency of the process. The output of the
381 hydrodynamic model consists of a set of inundation simulations that include several hazard intensity
382 variables in relation to flood extent: water depth, flow velocity, and duration of submersion. ESL scenarios
383 are then summarized into static maps, each one representing the maximum value reached by hazard
384 intensity variables during the simulated event at about 1 meter resolution. The flood extents corresponding
385 to each RP scenario are shown for Rimini (Figure 76) and Cesenatico (Figure 87).



386

387 **Figure 776.** Rimini, extent of land affected by flood according to frequency of occurrence of ESL event up to
 388 2100 for the baseline [left] and the defended scenario [right]. Basemap © Google Maps 2020.

389 In Rimini, the *Parco del Mare* barrier produces benefits in terms of avoided damage in the south-eastern part
 390 of the town (high-density area) for ESL events with a return period of 100 years or less. The north-western
 391 part and the marina are outside of the defended area; these areas are therefore subject to a similar amount of
 392 flooding across scenarios. In all the simulations, the buildings located behind the marina are the firsts to be
 393 flooded. In fact, the new and the old port channels located on both sides of the marina represent a hazard
 394 hotspot: as shown in the maps, the failure of the eastern channel, which has a relatively low elevation, is
 395 likely to cause the water to flood the eastern part of the town, even during inundation events that would not
 396 surpass the beach. In the defended scenarios, where both the coastal and the canal barriers are enabled, the
 397 flood extent in the south-eastern urban area becomes almost zero for ESL events with a probability of once in
 398 100 years, even when accounting for SLR up to 2100. Under the most exceptional ESL conditions (RP 250 in
 399 2100), the barrier is overtopped, generating a flood extent similar to the baseline scenario for the same
 400 occurrence probability.



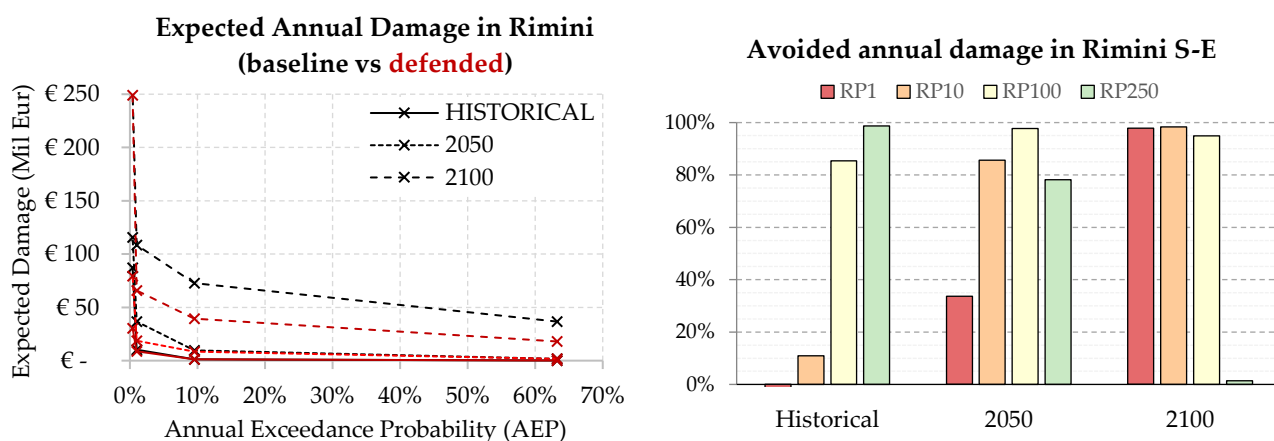
401

402 **Figure 887.** Cesenatico, extent of land affected by flood according to frequency of occurrence of ESL event up
 403 to 2100 for the baseline [left] and the defended scenario [right]. Basemap © Google Maps 2020.

404 In Cesenatico, a barrier designed similarly to *Parco del Mare* could provide significant reduction of flood
 405 extents under most hazard scenarios. Its effectiveness would be greater than in Rimini thanks to the
 406 complementary movable barrier system in use, which seals the port channel allowing to wall off the whole
 407 coastal perimeter, reducing the chance of water ingression in the urban area. In contrast, the erodible winter
 408 dune in the baseline defense scenario can only hold the heavy sea for shorter, less intense ESL events (RP 1 –
 409 10 years), and becomes ineffective with more exceptional, long-lasting events; from 2050 on, the winter dune
 410 could be surmounted and dismantled by sea waves even during frequent events (RP 1 year).

411 4.2 Expected Annual Damage

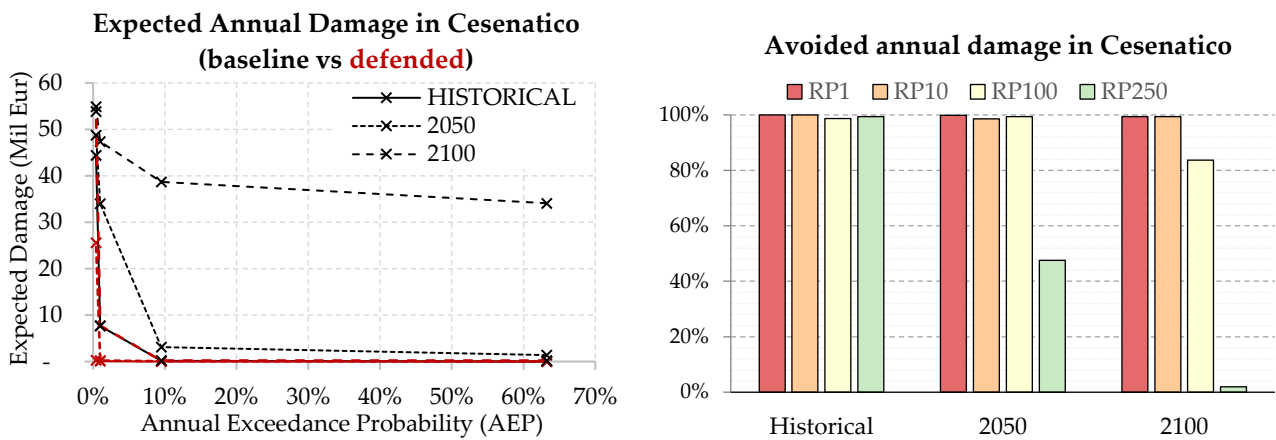
412 The Expected Annual Damage is calculated as a function of maximum exposed value and water depth. In
 413 Rimini, the EAD grows from around 650 thousand Eur under historical conditions to 2.8 million Eur in 2050
 414 and more than 32.3 million Eur in 2100. Under less severe ESL scenarios (RP below 100 years), the risk
 415 remains mostly confined around the marina, which is located outside the defended area, producing an
 416 expected damage below 10 thousand Eur. Under more extreme ESL scenarios, the benefits of the *Parco del*
 417 *Mare* project protecting the southern part of Rimini become more evident, avoiding about 65% of the
 418 expected damages in the defended scenarios compared to the undefended ones. The damage avoided in the
 419 defended scenarios grow almost linearly with the increase of the baseline EAD under future projections of
 420 sea level rise: under the defended scenario, the EAD is reduced on average by 45% in comparison with the
 421 undefended scenario (Figure 899, left). The project produces benefit up to scenario RP 250 years in 2100,
 422 where a projected TWL of 3.5 meters would cause the overtopping of the barrier, reducing the benefits to
 423 almost zero (Figure 89, right).



424
 425 **Figure 98.** Rimini: Expected Annual Damage (EAD) according to undefended scenario up to 2100, all town
 426 considered [left]; EAD reduction in the south-eastern part of the town thanks to hazard mitigation offered by
 427 the coastal barrier [right].

428 In Cesenatico, the average EAD for the undefended scenario grows from around 270 thousand Eur under
 429 historical conditions, to 1.7 million Eur in 2050 and almost 26 million Eur in 2100. In our simulations, the
 430 designed defence structure (a static barrier with height of 2.8 m along 7.8 km of coast) is able to avoid most
 431 of the damage inflicted to residential buildings (Figure 109, left). The measure becomes less efficient for the
 432 most extreme scenarios in 2050 and 2100, when the increase in TWL causes the surmounting of the barrier
 433 (Figure 910, right). This assessment does not account for the impacts over those beach resorts and bathing

434 facilities which are located along the barrier or between the barrier and the sea, and thus are equally exposed
 435 in both the baseline and the defended scenario; they would likely represent an additional 7-25% of the
 436 baseline damage.

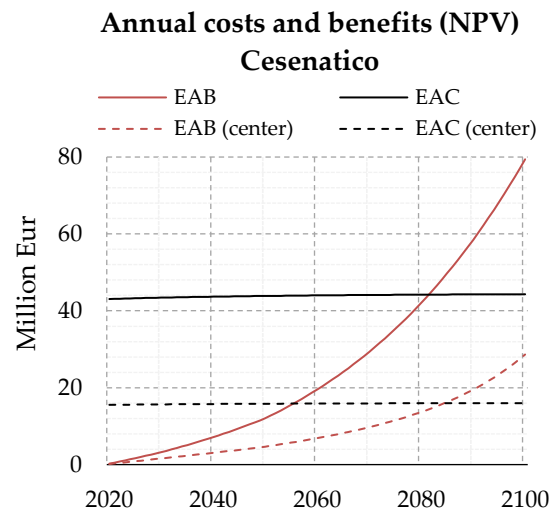
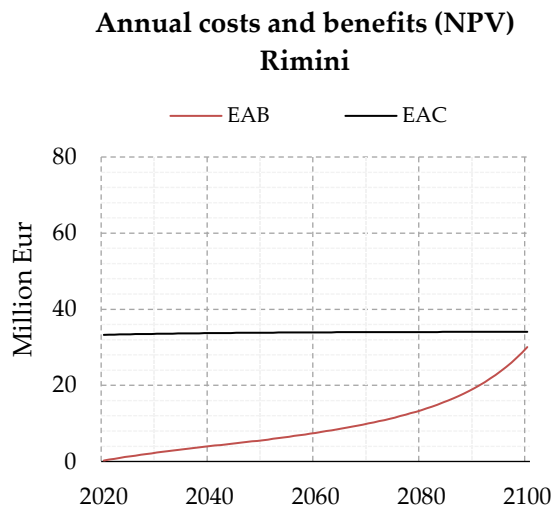


437
 438 **Figure 10109.** Cesenatico: Expected Annual Damage (EAD) according to undefended scenario up to 2100
 439 [left]; EAD reduction thanks to hazard mitigation offered by the coastal barrier [right].

440 **4.3 Cost-Benefit Analysis**

441 The estimates of avoided direct flood impacts are accounted in a DRR-oriented CBA to evaluate the
 442 feasibility of mitigation measures in terms of NPV, BCR and payback period for the two time-horizons (2021-
 443 2050: 30 years; and 2021-2100: 80 years). The assessment does not measure the indirect benefits brought in
 444 terms of urban renovation, which are the primary focus of the *Parco del Mare* project, measuring, instead,
 445 only the direct benefits in terms of direct flood damage reduction. In [Figure 1110](#), the Expected Annual
 446 Benefits (EAB) grow at faster rate approaching 2100 in both sites, because of the larger expected damages
 447 from more intense, less frequent flood events. The cost of defence implementation is repaid by avoided
 448 damage after about 40 years in Cesenatico and after 90 years in Rimini. At 2100, the BCR is 0.9 for Rimini
 449 and 1.8 for Cesenatico. These results clearly indicate an overall profitability of the defence structure
 450 implementation over the long term for Cesenatico. For the case of the municipality of Rimini, further
 451 investigation is required in order to account for the non-DRR benefits of the seafront renovation project. For
 452 instance, the potential reduction in indirect losses in terms of capital and labour productivity due to less
 453 frequent and less intense flooding events, and the potential increase in tourism and well-being of citizens
 454 due to renewed urban landscape, are factors that could be accounted for in a holistic CBA analysis and
 455 would likely return a shorter payback period.

456 In order to better understand the potential benefits of the mitigation measures over different areas of the two
 457 municipalities, we compare the results in terms of CBR over a selection of exposed records corresponding to
 458 the town higher-density area (i.e. Cesenatico historical center). Table 2 summarizes the metrics of the
 459 assessment for different area extent selections. Results do not differ much when comparing the CBA over
 460 different areas. In Cesenatico benefits grow proportionally to costs, so that the payback time does not change
 461 when considering a section of the town or the whole coastal perimeter.



462

463 **Figure 111110.** Cumulated flood defence costs and expected benefits at Net Present Value for Rimini (left)
 464 and Cesenatico (right).

465

466

467 **Table 2.** Summary of CBA for planned or designed seaside defence project in Rimini (all town and south
 468 section only) and Cesenatico (all town and center only) over a time horizon of 30 and 80 years (2021 to 2050
 469 and 2021 to 2100).

Metrics	Rimini				Cesenatico			
	All town		South only		All town		Center only	
	2050	2100	2050	2100	2050	2100	2050	2100
Baseline EAD [M EUR]	2.8	32	0.5	14.6	1.7	25.9	0.5	12.4
Defended EAD [M EUR]	2.4	17	0.1	0.9	0.1	0.4	0.1	0.4
Expected Annual Benefits [M EUR]	0.3	15	0.4	13.7	1.6	25.5	0.4	11.9
Sum of EAB (discounted) [M EUR]	5.6	30	4.1	27.8	12.0	79.4	4.7	28.6
Sum of EAC (discounted) [M EUR]	33.8	34.0	33.8	34.0	43.8	44.3	15.8	16.0
Net Present Value [M EUR]	-28.3	-4.0	-29.8	-6.3	-31.8	35.1	-11.24	12.6
Benefit-Cost ratio [-]	0.16	0.88	0.12	0.81	0.28	1.79	0.30	1.79

470 5. Conclusion

471 In this study we addressed coastal inundation risk scenarios over two coastal towns located along the North
 472 Adriatic coastal plain of Italy, which is projected to become increasingly exposed to ESL events due to
 473 changes in MSL induced by SLR and local subsidence phenomena. Both locations are expected to suffer
 474 increasing economic losses from these events, unless effective coastal adaptation measures are put in place.
 475 To understand the upcoming impacts and the potential benefits of designed coastal projects, we run a CBA
 476 comparing the baseline and the defended scenario in terms of flood losses over residential buildings, which
 477 represent the largest share of exposed buildings' footprints (93%). The defended scenario accounts for the
 478 effect of a coastal barriers based on the design of *Parco del Mare*, an urban renovation project under
 479 construction in Rimini. The same type of defence structure is envisaged along the coastal perimeter of the
 480 nearby town of Cesenatico. First, we characterised reference ESL events in terms of frequency and intensity
 481 based on local historical observations; then, we projected ESL scenarios to 2050 and 2100, accounting for the
 482 combined effect of eustatic-SLR and subsidence rates on the TWL, as obtained from existing local studies.
 483 We produced flood hazard maps estimating maximum flood extent and water depth using a high-resolution
 484 hydrodynamic model able to replicate the physics of the inundation process. The hazard maps were fed to a
 485 locally-calibrated damage model in order to calculate the expected annual damage for both baseline and
 486 defended scenarios. An increase in damage is expected for both urban areas from 2021 to 2100: in Cesenatico
 487 the EAD grows by a factor 96, in Rimini by a factor 49.

488 The results obtained from the CBA on both locations show growing profitability of present project
 489 investment over time, associated with the increase of damage triggered by intense ESL events: the EAD
 490 under the baseline hypothesis is expected to increase by 3.5-fold in 2050, up to 10-fold in 2100. The benefits
 491 brought by the coastal defence project become much larger in the second half of the century: the EAB grows
 492 6.1-fold in Rimini, 6.5-fold in Cesenatico, from 2050 to 2100. Avoided losses are expected to match the project
 493 implementation costs after about 40 years in Cesenatico and 90 years in Rimini. Benefits are found to
 494 increase proportionally to costs; the payback period in Cesenatico is the same considering either an
 495 investment on the protection of the whole town or only part of it. Further assessments of these renovation
 496 projects should look to measure the indirect and spill-over effects over the local economy brought by the
 497 project, possibly accounting also for the intangible benefits and scenarios of exposure change. The results are
 498 calculated in relation to emission scenario RCP 4.5; compared to RCP 8.5 at 2050, the difference in SLR
 499 contribution is negligible (~0.05 m), while at 2100, the difference between the two emission scenarios is larger
 500 (around 0.2 m), thus additional scenario analysis is suggested in future research.

501 **Data availability**

502 Mattia Amadio, & Arthur H. Essenfelder. (2021). Coastal flood inundation scenarios over Cesenatico and
503 Rimini: hazard and risk for Business as Usual and Defended options [Data set]. Hosted by Zenodo:
504 <https://zenodo.org/record/4783443>

505 **Authors contribution**

506 MA, AHE and SB conceptualized the study and designed the experiments. AHE carried out the coastal
507 hazard modelling. SR advised the model setup and calculation. SB and PM provided required data and
508 expertise about the case study areas. MA performed the economic risk modelling and wrote the manuscript.
509 SM supported the CBA calculations. JM and SB managed the funding acquisition and project supervision.
510 All co-authors have reviewed the manuscript.

511 **Acknowledgment**

512 The research leading to this paper received funding through the projects CLARA (EU's Horizon 2020
513 research and innovation programme under grant agreement 730482), SAFERPLACES (Climate-KIC
514 innovation partnership) and EUCP – European Climate Prediction system under grant agreement 776613.
515 We want to thank Luisa Perini for her kind support.

516 **References**

- 517 Amadio M, Scorzini AR, Carisi F, et al (2019) Testing empirical and synthetic flood damage models: the case
518 of Italy. *Nat Hazards Earth Syst Sci* 19:661–678 . doi: 10.5194/nhess-19-661-2019
- 519 Antonioli F, Anzidei M, Amorosi A, et al (2017) Sea-level rise and potential drowning of the Italian coastal
520 plains: Flooding risk scenarios for 2100. *Quat Sci Rev* 158:29–43 . doi: 10.1016/j.quascirev.2016.12.021
- 521 Armaroli C, Ciavola P, Perini L, et al (2012) Critical storm thresholds for significant morphological changes
522 and damage along the Emilia-Romagna coastline, Italy. *Geomorphology* 143–144:34–51 . doi:
523 10.1016/j.geomorph.2011.09.006
- 524 Armaroli C, Duo E (2018) Validation of the coastal storm risk assessment framework along the Emilia-
525 Romagna coast. *Coast Eng* 134:159–167 . doi: 10.1016/j.coastaleng.2017.08.014
- 526 ARPAE (2019) Relazione tecnica mappe della pericolosità e del rischio di alluvioni in ambito costiero
- 527 Boardman AE, Greenberg DH, Vining AR, Weimer DL (2018) *Cost-Benefit Analysis*. Cambridge University
528 Press
- 529 Bonaduce A, Pinardi N, Oddo P, et al (2016) Sea-level variability in the Mediterranean Sea from altimetry
530 and tide gauges. *Clim Dyn* 47:2851–2866 . doi: 10.1007/s00382-016-3001-2
- 531 Boon JD (2004) *Secrets of the Tide: Tide and Tidal Current Analysis and Predictions, Storm Surges and Sea*
532 *Level Trends*. Elsevier Inc.
- 533 Bos F, Zwaneveld P (2017) *Cost-Benefit Analysis for Flood Risk Management and Water Governance in the*
534 *Netherlands: An Overview of One Century*. SSRN Electron J. doi: 10.2139/ssrn.3023983
- 535 Bouwer LM (2011) Have disaster losses increased due to anthropogenic climate change? *Bull Am Meteorol*
536 *Soc*. doi: 10.1175/2010BAMS3092.1
- 537 Carbognin L, Teatini P, Tomasin A, Tosi L (2010) Global change and relative sea level rise at Venice: What
538 impact in term of flooding. *Clim Dyn* 35:1055–1063 . doi: 10.1007/s00382-009-0617-5

- 539 Carbognin L, Teatini P, Tosi L (2009) The impact of relative sea level rise on the Northern Adriatic Sea coast,
540 Italy. *WIT Trans Ecol Environ* 127:137–148 . doi: 10.2495/RAV090121
- 541 Carminati E, Martinelli G (2002) Subsidence rates in the Po Plain, northern Italy: the relative impact of
542 natural and anthropogenic causation. *Eng Geol* 66:241–255 . doi: 10.1016/S0013-7952(02)00031-5
- 543 Church JA, White NJ (2011) Sea-Level Rise from the Late 19th to the Early 21st Century. *Surv Geophys*
544 32:585–602 . doi: 10.1007/s10712-011-9119-1
- 545 Ciavola P, Coco G (eds) (2017) *Coastal storms: processes and impacts*. Wiley-Blackwell
- 546 Comune di Rimini (2018) *Parco del Mare Sud - Strategia per la rigenerazione urbana*
- 547 Comune di Rimini (2019a) *Deliberazione originale di giunta comunale N. 99 del 11/04/2019*
- 548 Comune di Rimini (2019b) *Deliberazione originale di giunta comunale N. 118 del 02/05/2019*
- 549 Comune di Rimini (2020) *Deliberazione originale di giunta comunale N. 128 del 26/05/2020*
- 550 Comune di Rimini (2021a) *Deliberazione originale di giunta comunale N. 19 del 19/01/2021*
- 551 Comune di Rimini (2021b) *Deliberazione originale di giunta comunale N. 20 del 19/01/2021*
- 552 CRESME (2014) *Definizione dei costi di (ri)costruzione nell’edilizia*
- 553 Familkhalili R, Talke SA, Jay DA (2020) Tide-Storm Surge Interactions in Highly Altered Estuaries: How
554 Channel Deepening Increases Surge Vulnerability. *J Geophys Res Ocean* 125:e2019JC015286 . doi:
555 10.1029/2019JC015286
- 556 Froehlich DC (2002) IMPACT Project Field Tests 1 and 2: “Blind” Simulation. 1–18
- 557 Fuhrmann CM, Wood KM, Rodgers JC (2019) Assessment of storm surge and structural damage on San
558 Salvador Island, Bahamas, associated with Hurricane Joaquin (2015). *Nat Hazards* 99:913–930 . doi:
559 10.1007/s11069-019-03782-2
- 560 Gambolati G, Giunta G, Putti M, et al (1998) Coastal Evolution of the Upper Adriatic Sea due to Sea Level
561 Rise and Natural and Anthropogenic Land Subsidence. 1–34 . doi: 10.1007/978-94-011-5147-4
- 562 Garnier E, Ciavola P, Spencer T, et al (2018) Historical analysis of storm events: Case studies in France,
563 England, Portugal and Italy. *Coast Eng* 134:10–23 . doi: 10.1016/j.coastaleng.2017.06.014
- 564 Geofabrik GmbH (2018) *OpenStreetMap data extracts*
- 565 Hallegatte S, Green C, Nicholls RJ, Corfee-Morlot J (2013) Future flood losses in major coastal cities. *Nat*
566 *Clim Chang*. doi: 10.1038/nclimate1979
- 567 Hinkel J, Lincke D, Vafeidis AT, et al (2014) Coastal flood damage and adaptation costs under 21st century
568 sea-level rise. *Proc Natl Acad Sci*. doi: 10.1073/pnas.1222469111
- 569 Huizinga J, Moel H De, Szewczyk W (2017) *Global flood depth-damage functions : Methodology and the*
570 *Database with Guidelines*
- 571 IPCC (2019) *IPCC Special Report on the Ocean and Cryosphere in a Changing Climate*
- 572 ISPRA (2012) *Mare e ambiente costiero. Temat Primo Piano - Annu dei dati Ambient 2011* 259–322
- 573 ISTAT (2011) *15° censimento della popolazione e delle abitazioni*
- 574 Jongman B, Kreibich H, Apel H, et al (2012a) Comparative flood damage model assessment: towards a
575 European approach. *Nat Hazards Earth Syst Sci* 12:3733–3752
- 576 Jongman B, Ward PJ, Aerts JCJH (2012b) Global exposure to river and coastal flooding: Long term trends
577 and changes. *Glob Environ Chang*. doi: 10.1016/j.gloenvcha.2012.07.004
- 578 Jonkman SN, Brinkhuis-Jak M, Kok M (2004) Cost benefit analysis and flood damage mitigation in the
579 Netherlands. *Heron* 49:95–111

- 580 Kain CL, Lewarn B, Rigby EH, Mazengarb C (2020) Tsunami Inundation and Maritime Hazard Modelling
581 for a Maximum Credible Tsunami Scenario in Southeast Tasmania, Australia. *Pure Appl Geophys*
582 177:1549–1568 . doi: 10.1007/s00024-019-02384-0
- 583 Kemp AC, Horton BP, Donnelly JP, et al (2011) Climate related sea-level variations over the past two
584 millennia. *Proc Natl Acad Sci U S A* 108:11017–11022 . doi: 10.1073/pnas.1015619108
- 585 Kind JM (2014) Economically efficient flood protection standards for the Netherlands. *J Flood Risk Manag*
586 7:103–117 . doi: 10.1111/jfr3.12026
- 587 Kirezci E, Young IR, Ranasinghe R, et al (2020) Projections of global-scale extreme sea levels and resulting
588 episodic coastal flooding over the 21st Century. *Sci Rep* 10:1–12 . doi: 10.1038/s41598-020-67736-6
- 589 Lambeck K, Antonioli F, Anzidei M, et al (2011) Sea level change along the Italian coast during the Holocene
590 and projections for the future. *Quat Int* 232:250–257 . doi: 10.1016/j.quaint.2010.04.026
- 591 Lambeck K, Purcell A (2005) Sea-level change in the Mediterranean Sea since the LGM: Model predictions
592 for tectonically stable areas. In: *Quaternary Science Reviews*. Pergamon, pp 1969–1988
- 593 Lionello P (2012) The climate of the Venetian and North Adriatic region: Variability, trends and future
594 change. *Phys Chem Earth* 40–41:1–8 . doi: 10.1016/j.pce.2012.02.002
- 595 Lionello P, Barriopedro D, Ferrarin C, et al (2020) Extremes floods of Venice: characteristics, dynamics, past
596 and future evolution. *Nat Hazards Earth Syst Sci* 1–34 . doi: 10.5194/nhess-2020-359
- 597 Lionello P, Conte D, Marzo L, Scarascia L (2017) The contrasting effect of increasing mean sea level and
598 decreasing storminess on the maximum water level during storms along the coast of the Mediterranean
599 Sea in the mid 21st century. *Glob Planet Change* 151:80–91 . doi: 10.1016/j.gloplacha.2016.06.012
- 600 Lowe J (2008) Intergenerational wealth transfers and social discounting: Supplementary Green Book
601 guidance. HM Treasury, London 3–6
- 602 Lowe J, Gregory J, Flather R (2001) Changes in the occurrence of storm surges around the United Kingdom
603 under a future climate scenario using a dynamic storm surge model driven by the Hadley Centre
604 climate models. *Clim Dyn* 18:179–188
- 605 Marsico A, Lisco S, Lo Presti V, et al (2017) Flooding scenario for four Italian coastal plains using three
606 relative sea level rise models. *J Maps* 13:961–967 . doi: 10.1080/17445647.2017.1415989
- 607 Masina M, Lamberti A, Archetti R (2015) Coastal flooding: A copula based approach for estimating the joint
608 probability of water levels and waves. *Coast Eng* 97:37–52 . doi: 10.1016/j.coastaleng.2014.12.010
- 609 McGranahan G, Balk D, Anderson B (2007) The rising tide: Assessing the risks of climate change and human
610 settlements in low elevation coastal zones. *Environ Urban*. doi: 10.1177/0956247807076960
- 611 McInnes KL, Walsh KJE, Hubbert GD, Beer T (2003) Impact of sea-level rise and storm surges in a coastal
612 community. *Nat Hazards* 30:187–207 . doi: 10.1023/A:1026118417752
- 613 Mechler R (2016) Reviewing estimates of the economic efficiency of disaster risk management: opportunities
614 and limitations of using risk-based cost–benefit analysis. *Nat Hazards* 81:2121–2147 . doi:
615 10.1007/s11069-016-2170-y
- 616 Melet A, Almar R, Hemer M, et al (2020) Contribution of Wave Setup to Projected Coastal Sea Level
617 Changes. *J Geophys Res Ocean* 125:e2020JC016078 . doi: 10.1029/2020JC016078
- 618 Meli M, Olivieri M, Romagnoli C (2021) Sea-level change along the emilia-romagna coast from tide gauge
619 and satellite altimetry. *Remote Sens* 13:1–26 . doi: 10.3390/rs13010097
- 620 Meyssignac B, Cazenave A (2012) Sea level: A review of present-day and recent-past changes and variability.
621 *J. Geodyn.* 58:96–109
- 622 Mitchum GT, Nerem RS, Merrifield MA, Gehrels WR (2010) Modern Sea-Level-Change Estimates. In:

- 623 Understanding Sea-Level Rise and Variability. Wiley-Blackwell, Oxford, UK, pp 122–142
- 624 Muis S, Verlaan M, Winsemius HC, et al (2016) A global reanalysis of storm surges and extreme sea levels.
625 Nat Commun 7:1–11 . doi: 10.1038/ncomms11969
- 626 Nicholls RJ, Cazenave A (2010) Sea-level rise and its impact on coastal zones. Science (80-) 328:1517–1520 .
627 doi: 10.1126/science.1185782
- 628 Olsen AS, Zhou Q, Linde JJ, Arnbjerg-Nielsen K (2015) Comparing methods of calculating expected annual
629 damage in urban pluvial flood risk assessments. Water (Switzerland) 7:255–270 . doi: 10.3390/w7010255
- 630 Peltier WR (2004) Global Glacial Isostasy and the surface of the ice-age Earth: the ICE-5G (VM2) Model and
631 GRACE. Annu Rev Earth Planet Sci 32:111–149 . doi: 10.1146/annurev.earth.32.082503.144359
- 632 Peltier WR, Argus DF, Drummond R (2015) Space geodesy constrains ice age terminal deglaciation: The
633 global ICE-6G_C (VM5a) model. J Geophys Res Solid Earth 120:450–487 . doi: 10.1002/2014JB011176
- 634 Perini L, Calabrese L, Deserti M, et al (2011) Le mareggiate e gli impatti sulla costa in Emilia-Romagna 1946-
635 2010
- 636 Perini L, Calabrese L, Lorito S, Luciani P (2015) Il rischio da mareggiata in Emilia-Romagna: l’evento del 5-6
637 Febbraio 2015. Geol 53:8–17
- 638 Perini L, Calabrese L, Luciani P, et al (2017) Sea-level rise along the Emilia-Romagna coast (Northern Italy) in
639 2100: Scenarios and impacts. Nat Hazards Earth Syst Sci 17:2271–2287 . doi: 10.5194/nhess-17-2271-2017
- 640 Perini L, Calabrese L, Salerno G, et al (2016) Evaluation of coastal vulnerability to flooding: Comparison of
641 two different methodologies adopted by the Emilia-Romagna region (Italy). Nat Hazards Earth Syst Sci
642 16:181–194 . doi: 10.5194/nhess-16-181-2016
- 643 Perini L, Calabrese L, Salerno G, Luciani P (2012) Mapping of flood risk in Emilia-Romagna coastal areas.
644 Rend Online Soc Geol Ital 21:501–502 . doi: 10.13140/2.1.1703.7766
- 645 Polcari M, Albano M, Montuori A, et al (2018) InSAR monitoring of Italian coastline revealing natural and
646 anthropogenic ground deformation phenomena and future perspectives. Sustain 10:4–7 . doi:
647 10.3390/su10093152
- 648 Price R (2018) Cost-effectiveness of disaster risk reduction and adaptation to climate change. 1–21
- 649 Roberts S (2020) ANUGA - Open source hydrodynamic / hydraulic modelling
- 650 Roberts S, Nielsen O, Gray D, Sexton J (2015) ANUGA User Manual
- 651 Scarascia L, Lionello P (2013) Global and regional factors contributing to the past and future sea level rise in
652 the Northern Adriatic Sea. Glob Planet Change 106:51–63 . doi: 10.1016/j.gloplacha.2013.03.004
- 653 Solari L, Del Soldato M, Bianchini S, et al (2018) From ERS 1/2 to Sentinel-1: Subsidence Monitoring in Italy
654 in the Last Two Decades. Front Earth Sci 6: . doi: 10.3389/feart.2018.00149
- 655 Stocker TF, Dahe Q, Plattner G-K, et al (2013) Technical Summary. In: Stocker TF, Qin D, Plattner G-K, et al.
656 (eds) Climate Change 2013: The Physical Science Basis. Contribution of Working Group I to the Fifth
657 Assessment Report of the Intergovernmental Panel on Climate Change. Cambridge University Press,
658 Cambridge, United Kingdom and New York, NY, USA., pp 33–115
- 659 Syvitski JPM, Kettner AJ, Overeem I, et al (2009) Sinking deltas due to human activities. Nat Geosci. doi:
660 10.1038/ngeo629
- 661 Teatini P, Ferronato M, Gambolati G, et al (2005) A century of land subsidence in Ravenna, Italy. Environ
662 Geol 47:831–846 . doi: 10.1007/s00254-004-1215-9
- 663 Teatini P, Ferronato M, Gambolati G, Gonella M (2006) Groundwater pumping and land subsidence in the
664 Emilia-Romagna coastland, Italy: Modeling the past occurrence and the future trend. Water Resour Res
665 42: . doi: 10.1029/2005WR004242

666 Tsimplis MN, Marcos M, Somot S (2008) 21st century Mediterranean sea level rise: Steric and atmospheric
667 pressure contributions from a regional model. *Glob Planet Change* 63:105–111 . doi:
668 10.1016/j.gloplacha.2007.09.006

669 Tsimplis MN, Raicich F, Fenoglio-Marc L, et al (2012) Recent developments in understanding sea level rise at
670 the Adriatic coasts. *Phys Chem Earth* 40–41:59–71 . doi: 10.1016/j.pce.2009.11.007

671 Tsimplis MN, Rixen M (2002) Sea level in the Mediterranean Sea: The contribution of temperature and
672 salinity changes. *Geophys Res Lett* 29:51-1-51-4 . doi: 10.1029/2002gl015870

673 Umgiesser G, Bajo M, Ferrarin C, et al (2020) The prediction of floods in Venice: methods, models and
674 uncertainty. *Nat Hazards Earth Syst Sci* 1–47 . doi: 10.5194/nhess-2020-361

675 Vousdoukas MI, Mentaschi L, Feyen L, Voukouvalas E (2017) Extreme sea levels on the rise along Europe’s
676 coasts. *Earth’s Futur* 5:1–20 . doi: 10.1002/ef2.192

677 Vousdoukas MI, Mentaschi L, Voukouvalas E, et al (2018) Global probabilistic projections of extreme sea
678 levels show intensification of coastal flood hazard. *Nat Commun* 9:1–12 . doi: 10.1038/s41467-018-
679 04692-w

680 Wöppelmann G, Marcos M (2012) Coastal sea level rise in southern Europe and the nonclimate contribution
681 of vertical land motion. *J Geophys Res Ocean* 117: . doi: 10.1029/2011JC007469

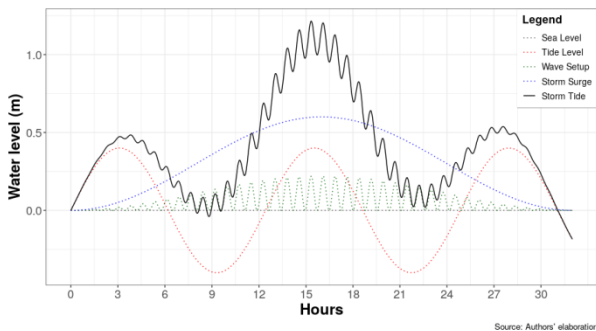
682 Zanchettin D, Bruni S, Raicich F, et al (2020) Review article: Sea-level rise in Venice: historic and future
683 trends. *Nat Hazards Earth Syst Sci Discuss* 1–56 . doi: 10.5194/nhess-2020-351

684 Zanchettin D, Traverso P, Tomasino M (2007) Observations on future sea level changes in the Venice lagoon.
685 *Hydrobiologia*. doi: 10.1007/s10750-006-0416-5

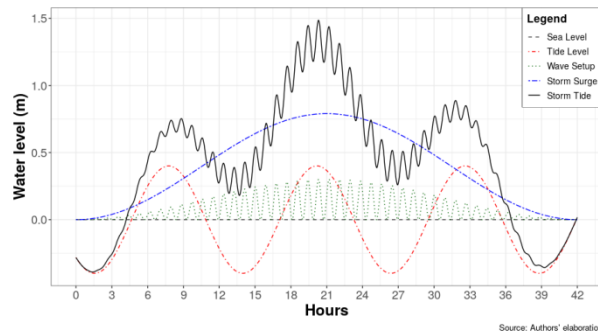
686

687 **Annex 1**

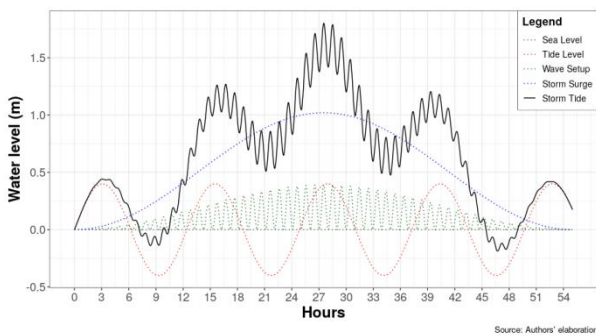
RP 1 year



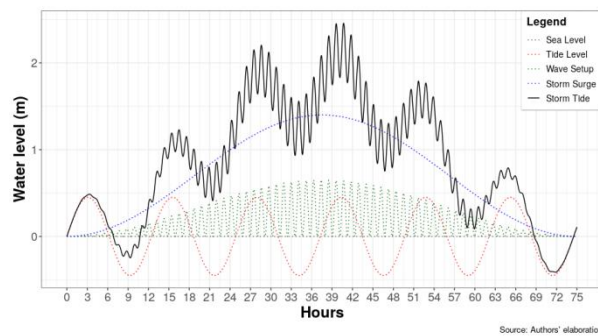
RP 10 years



RP 100 years



RP 250 years

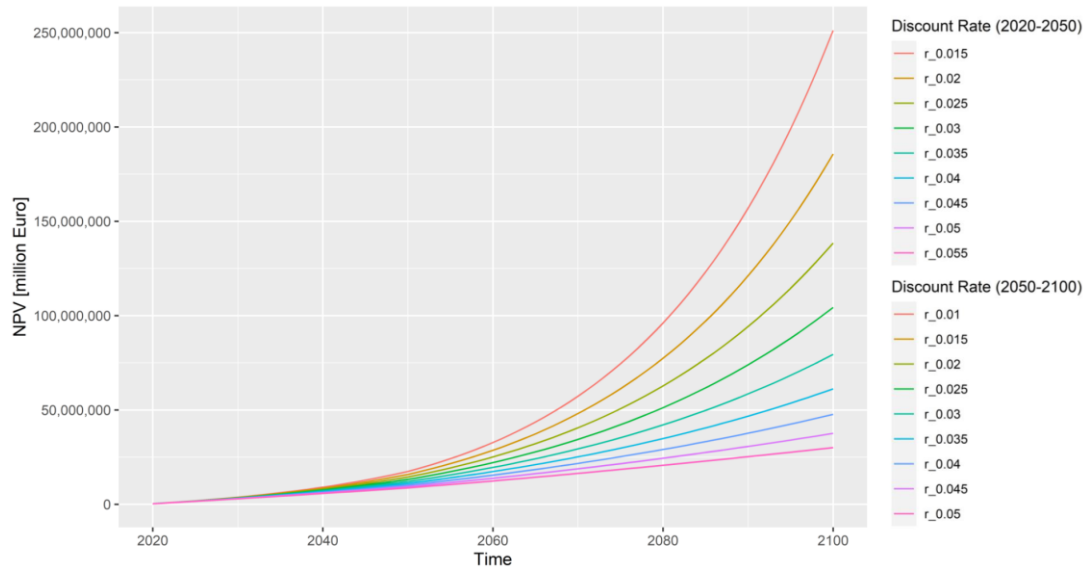


688 [Figure A1](#). Dynamic boundary conditions for simulating theoretical storm surge events in ANUGA. [Total](#)
689 [Water Level](#) (black) as a sum of tide (red), storm surge (blue) and wave setup (green) for all simulated ESL
690 [scenarios](#) (Return Period of once-in-1, 10, 100 and 250 years).

691

692 [Annex 12](#)

693 A sensitivity analysis is carried out on the discount rate. [Figure A12](#) below shows how the NPV changes
694 with discount rate r ranging from 1.5% to 5.5% (2020 to 2050) and 1% to 5% (2050-2100).



695

696 [Figure A21](#). Sensitivity analysis of NPV using a variable discount rate.